JOURNAL OF MATERIALS SCIENCE 8 (1973) 581–589

The sputtering of rough cylinders; applications to the thinning of fibres for transmission electron microscopy

P. J. GOODHEW
Department of Metallurgy and Materials Technology, University of Surrey, Guildford, UK

Thinning by ion-bombardment is a useful technique for the preparation of carbon and other fibres for transmission electron microscopy. It is shown that the presence of axial ridges on the initial fibre leads to the development of striations perpendicular to the axis of the thinned specimen. An analysis of the variation of ion incidence angle on a rotating cylinder enables the change in shape of a fibre on sputtering to be explained; scanning electron microscopy of sputtered fibres confirms these conclusions. A mechanism for the formation of striations perpendicular to pre-existing ridges on the fibre is proposed.

1. Introduction

Ion-bombardment has recently been used for polishing [1], etching [2, 12], surface cleaning and thinning specimens for transmission electron microscopy [2-4]. Because of the dependence of erosion rate on lattice orientation much of the work of thinning for electron microscopy has been carried out on non-crystalline or single crystal materials. Even in these cases, however, many workers have noticed the development of surface structures ("ripples", "dunes" or "furrows") on plane surfaces [e.g., 2, 5, 17] and the formation of cones at heterogeneities on otherwise plane surfaces [6, 7].

Many of these features have been successfully explained in terms of the variation of sputtering yield with angle of ion incidence and have been shown to arise from initially small irregularities in the surface [8-11, 17]. From these considerations three surface geometries have been shown to be stable on a homogeneous solid under ion-bombardment. These are a plane perpendicular to the ion beam, a plane parallel to the ion beam and a third plane at an angle depending on the sputtering characteristics of the material and its crystal geometry [10, 18]. However, the development of these stable configurations may require the removal of a great deal of material from the bombarded surface and this situation may not be attained in a real experiment [10]. Very few experiments have been carried out on specimens which were not initially approximately planar, although Wehner [6] has sputtered small single crystal metal spheres and has observed their development into cones.

In the application of ion-beam thinning to the preparation of thin specimens for TEM the tendency to develop surface structures is clearly highly undesirable. In order to reduce this to a minimum it has been common to rotate the specimen within its own plane while bombarding with, for example, argon ions at an angle of incidence between 60 and 85°. These conditions prevent the formation of cones on plane specimens but do not entirely remove surface "ripple" which manifests itself as slight variations in thickness of the TEM specimen [17]. This has proved satisfactory for a wide range of crystalline and amorphous materials which are available in thin sheets. However, in the course of investigations into the microstructure of carbon fibres it has been necessary, both in our laboratories and at Harwell [13], to thin single fibres for transmission electron microscopy. Ion-bombardment provides the most easily controlled way of doing this and is suitable for use on a wide range of fibre types. Early results from high-modulus fibres showed, however, that although long regions of the fibres could be made electron-transparent, prominent striations appeared across the axis of the fibre [14, 15]. An example is shown in Fig. 1. It was thought unlikely that these reflected a real variation in microstructure over such a long period (0.1 to

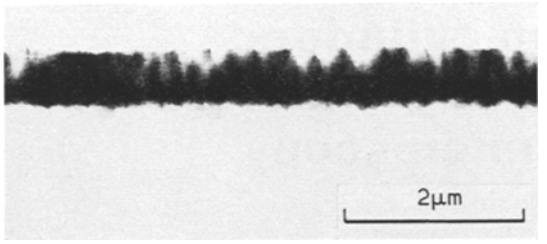

Figure 1 High modulus PAN-based carbon fibre thinned by argon-ion bombardment (5 kV).

1 μm) and hence experiments were devised to establish whether they arose from the ion-sputtering mechanism. This paper describes experiments with fibres of the same material but with differential initial morphologies and presents an explanation of the development of striations.

2. Experimental techniques

2.1. Materials

The carbon fibres used were of two basic types. Initial experiments were carried out on fibres from polyacrylonitrile (PAN) precursors; these were either Morganite Modmor fibres (Type 1) or fibres prepared in our laboratories. These fibres all show surface ridges running parallel to the fibre axis (Fig. 4a). Later experiments were carried out using fibres from pitch which also have a circular cross-section but show a very smooth surface (Fig. 5a).

2.2. Ion-bombardment

All the bombardments were carried out in a standard Edwards Instruments IBMA 1 thinning unit. Argon, nitrogen or oxygen ions were used at 5 kV. The fibres, two or three at a time, were mounted using a colloidal silver suspension across TEM specimen grids having a single large hole (Fig. 2). The specimen grid was similarly fixed to the larger specimen-retaining disc in the ion thinning unit. The fibres could be bombarded from one or both sides and were always held such that the angle of ion incidence on the disc was 65° (Fig. 3). The specimens were rotated about the axis shown in Fig. 3, except for a static experiment in which the fibre was held stationary in the plane of the diagram (Fig. 3).

2.3. Observations

After ion-bombardment the whole specimen-retaining disc, with the grid and fibres still stuck to it, was placed in a Stereoscan IIA for surface

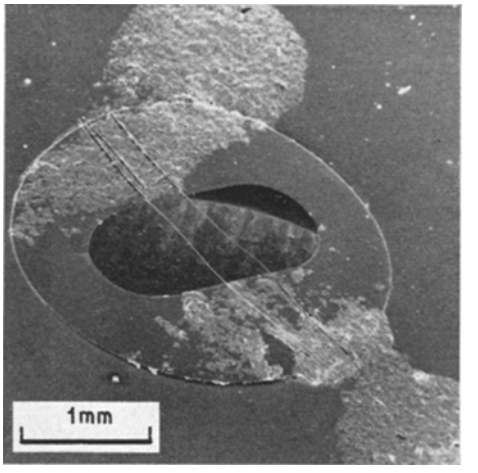

Figure 2 A single-hole electron microscope grid with two fibres mounted for ion-thinning. The lighter areas are colloidal silver used to attach the fibres to the grid and the grid to its mount.

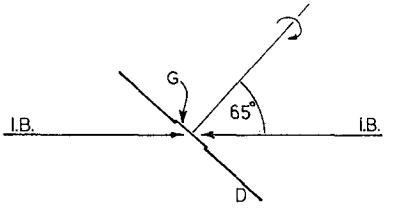

Figure 3 The geometry of ion-bombardment in the thinning unit. G – grid carrying fibres, D – specimen mounting disc, I.B. – ion beams.

examination. This was generally carried out at 20 kV but the usual problems associated with SEM images from cylinders were met, contrast being lost due to excess brightness at the edges of the fibre which is at a glancing angle to the electron beam. Consequently, much use was made of a differential signal, which eliminates gross variation in overall contrast. Unfortunately it also reduces considerably the three-dimensional appearance of the image and therefore we have presented many micrographs with half the image viewed in a conventional secondary electron mode and the other half viewed with the derivative of the same signal (e.g. Figs. 5, 7 and 13). This is very easy to record on the SEM since the intensities of the two images may be set separately and once the correct settings for photography have been established a single photograph can be taken and the derivative signal switched on half-way through the scan. A single negative carrying both types of image results.

Those fibres required for transmission micro-

scopy were examined in a JEOL JEM 100B at 100 keV. The specimen grid bearing the fibres was prised off the retaining disc with tweezers and mounted directly in the TEM specimen holder.

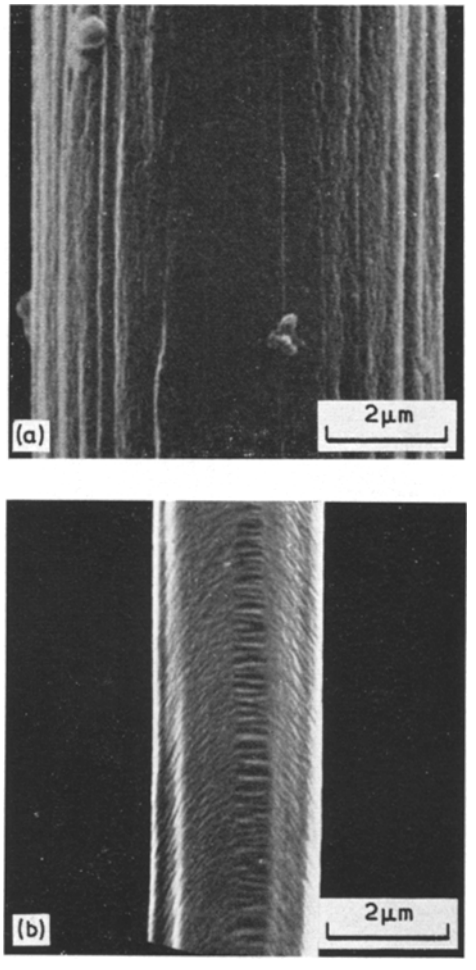

Figure 4 A PAN-based carbon fibre (a) before bombardment and (b) after 28 h of bombardment with 5 kV nitrogen ions.

3. Structures observed

3.1. PAN-based fibres

It is immediately apparent in the scanning electron microscope that the striations observed by TEM are in fact variations in thickness of the fibre due to the development of surface striations during thinning (Fig. 4a and b). What is surprising is that the striations develop perpendicular to the pre-existing ridges on the fibres. This would be most easily understood if there were a real structural variation in the fibre on the scale of the observed striations. However, the known crystallite structure is on a far smaller scale (< 10 nm) and there is no evidence from any other source (e.g., X-ray scattering) to suggest a structure of period 100 nm or greater.

Most of our work has been performed on these PAN-based fibres and in an attempt to find the most suitable thinning conditions, two alternative gases were used as well as argon. Nitrogen and oxygen were chosen since they are of similar atomic weight (less than half that of argon) but whereas nitrogen would be expected to be inert to the carbon, oxygen could enter into reactions and possibly give a different etching effect.

The only difference observed in practice has been that the lighter ions sputter at a lower rate so that at typical ion-beam currents of about 50 μA per gun several tens of hours were needed to thin a fibre to perforation using the lighter gases. Using argon we normally perforate an 8 μm diameter fibre in 8 to 10 h at 50 μA per gun. Exact quantitative comparisons are difficult since the ion current often varies during a single run and we have no monitoring facilities.

3.2. Pitch-based fibres

Carbon fibres made from pitch generally have a circular cross-section and an extremely smooth surface. Although the fibres we used were initially of a larger diameter than the PAN-based fibres (~ 12 μm against ~ 8 μm) the two types were considered to be sufficiently similar in all respects but surface topography. The effect of ion-thinning a smooth fibre is shown in Fig. 5. It can be seen that although there is evidence of facetting, the fibre surface is as smooth as it was initially and there is no evidence of the formation of striations. Transmission micrographs (e.g., Fig. 6) shows that although there are no coarse striations there is a fine surface "ripple", similar to those seen on planar sputtered surfaces. This however does not unduly interfere with transmission microscope observations, as long as it is recognized as an artefact.

3.3. Flame-polished PAN-based fibres

There are undoubtedly microstructural differences between the PAN-based and pitch-based fibres and it was therefore thought desirable to confirm that the striations were caused by axial ridges by an independent experiment. Coyle *et al* [16] have shown that carbon fibres can be thinned by rapid oxidation in an oxy-hydrogen

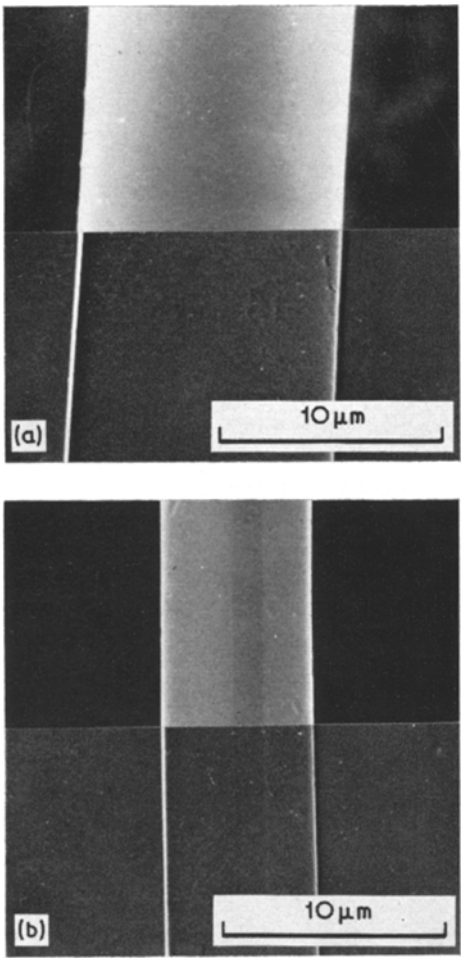

Figure 5 A pitch-based carbon fibre (a) before bombardment and (b) after 8 h of bombardment with 5 kV argon ions. Scanning electron micrographs; top half is secondary electron image, lower half is differentiated.

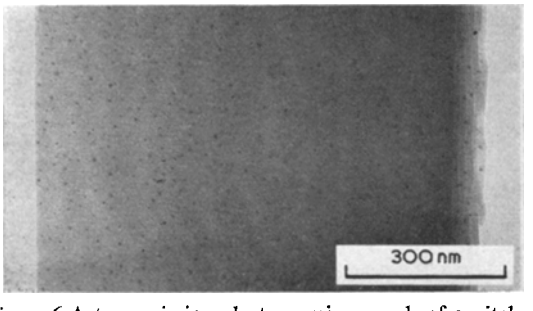

Figure 6 A transmission electron micrograph of a pitch-based carbon fibre thinned by argon-ion bombardment, showing a surface "ripple". Fibre axis vertical.

flame. Our PAN-based fibres were polished very briefly in this way in order to remove the surface ridges, with the result shown in Fig. 7a. It can be seen that although the surface is not absolutely smooth the regular axial ridges have disappeared. These polished fibres were then mounted and ion-thinned in the same way as other fibres, until perforation occurred (Fig. 7b). It is evident that although a few surface features persist no striations are visible. This is confirmed by transmission microscopy (Fig. 8).

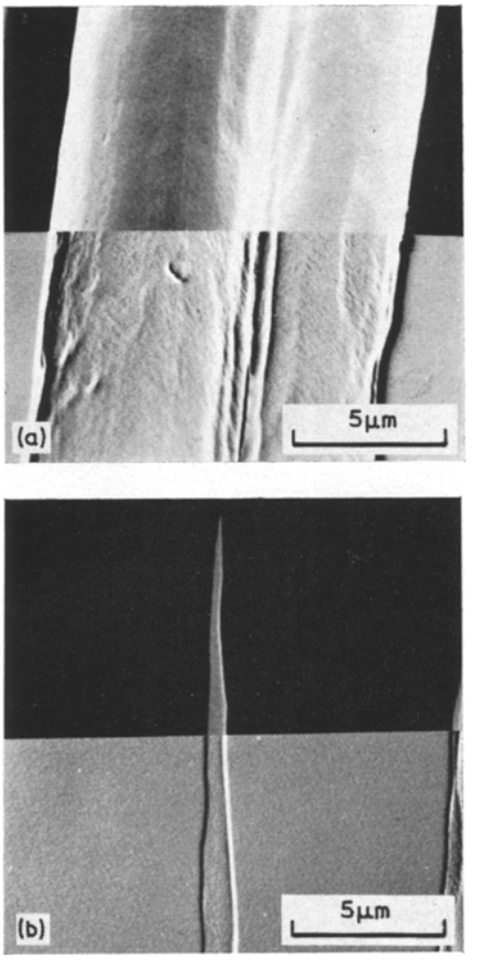

Figure 7 (a) Two PAN-based carbon fibres after flame-polishing. (b) A single flame-polished fibre after subsequent ion-thinning to perforation. Scanning electron micrographs; top half is secondary electron image, lower half is differentiated.

4. Discussion

All the above experiments have been carried out with the specimens rotating about the axis perpendicular to the plane of the specimen grid

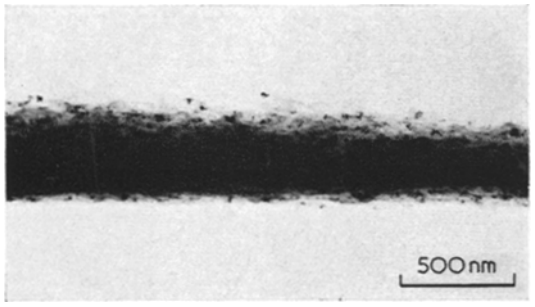

Figure 8 A transmission electron micrograph of a flame-polished, ion-thinned PAN-based fibre. Compare with Fig. 1.

(see Fig. 3). The structures developed on ion-thinning clearly depend on the geometry of ion incidence on the fibre surface, since sputtering rate is strongly dependent on angle of incidence θ. (Figs. 9 and 10.) In the next sections the variation of angle of incidence as the specimen rotates is considered and the effect of this on the shape of a sputtered smooth cylinder is discussed; subsequently the effect of axial ridges on the cylinder is considered.

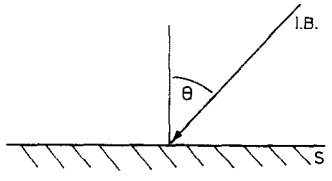

Figure 9 The definition of the angle of ion incidence, θ. I.B. – ion beam, S – sputtered surface.

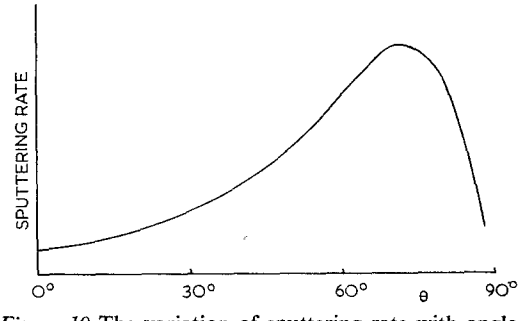

Figure 10 The variation of sputtering rate with angle of ion incidence (schematic).

4.1. Geometry of ion incidence

The angular parameters required to define the position of a fibre in the ion-thinning unit with respect to the ion beam are illustrated in Fig. 11. The fibre is represented by a cylinder; the angle β corresponds to the angle of tilt of the specimen holder in the ion-thinning unit (always 25° in our experiments); the angle α defines the angle of rotation of the fibre about the axis and the angle γ defines the position on the fibre of the point under consideration. Over the length of fibre being considered the ion beam is effectively uniform and parallel so that all points along the length of the fibre defined by γ are treated as equivalent.

It can be calculated by vector methods (see Appendix) that

$$\cos\theta = -\sin\beta\cos\gamma - \cos\alpha\cos\beta\sin\gamma\,.$$

Since in all our experiments β was held constant at 25° it is possible to plot a table of values of θ at 10° intervals of α and γ. This is shown in Table I, together with the angle ϕ between the ion beam and the axis of the fibre, which is clearly independent of γ. Several qualitative inferences can be drawn from this table: if we assume that the sputtering rate for angles of ion incidence (θ) between 60 and 80° is greater than that for other angles we can establish which parts of the fibre will be eroded preferentially. The appropriate regions are shown hatched in Table I. It can be seen that the regions of fibre around $\gamma = 0$ and 180° spend virtually all their time (while rotating) at a favourable angle for sputtering whereas those around $\gamma = 90°$ spend very little time at these angles. We can therefore predict that the fibre should develop from a circular cross-section towards the more complex shape shown in Fig. 12. This is borne out in general terms by the observation shown in Figs. 4b and 5b.

4.2. Formation of striations

It is well known that striated structures can arise on ion-bombarded polycrystalline material when the angle of ion incidence is very high, i.e. at glancing incidence [e.g. 12]. This is undoubtedly true in the present case as the micrographs of a fibre bombarded in a static position $\alpha = 90°$ show (Fig. 13). However, when the fibre is rotated, glancing incidence ($\theta \sim 90°$C) occurs over much of the fibre surface, as is shown by the area between the hatched areas in Table I. For the parts of the fibre which spend a long time at glancing ion incidence (γ = 20 to 30° and 150 to 160° initially) the angle between the ion beam and fibre axis (ϕ) is varying rapidly between $\sim$ 40 and 90°. This would at first sight seem to be

TABLE I The values of θ and ϕ as a function of α and γ with $\beta = 25°$.

ϕ	α \ γ	0	10	20	30	40	50	60	70	80	90	100	110	120	130	140	150	160	170	180
90	0	65	55	45	35	25	15	5	5	15	25	35	45	55	65	75	85	95	105	115
81	10	65	55	45	36	26	17	10	10	18	27	36	46	56	66	76	85	95	105	115
72	20	65	56	46	38	29	22	18	19	24	32	40	49	58	68	77	87	96	106	115
63	30	65	56	48	41	34	29	27	28	32	38	46	54	62	71	80	88	97	106	115
54	40	65	58	51	45	40	37	36	37	41	46	52	60	67	75	83	91	99	107	115
46	50	65	59	53	49	46	44	44	46	50	54	60	66	73	80	87	94	101	108	115
38	60	65	60	56	54	52	52	53	55	59	63	68	74	80	86	92	98	104	110	115
32	70	65	62	60	59	58	59	61	64	68	72	77	82	87	92	97	102	107	111	115
27	80	65	64	63	64	65	67	70	73	77	81	85	90	94	99	103	107	110	113	115
25	90	65	65	67	69	71	74	78	82	86	90	94	98	102	106	109	111	113	115	115
27	100	65	67	70	73	77	81	86	90	95	99	103	107	110	113	115	116	117	116	115
32	110	65	69	73	78	83	88	93	98	103	108	112	116	119	121	122	121	120	118	115
38	120	65	70	76	82	88	94	100	106	112	117	121	125	127	128	128	126	123	120	115
46	130	65	72	79	86	93	100	107	114	120	126	130	134	136	136	134	131	127	121	115
54	140	65	73	81	89	97	105	113	120	128	134	139	143	144	143	140	135	129	122	115
63	150	65	74	83	91	100	109	118	126	134	142	148	152	153	151	146	139	132	123	115
72	160	65	74	84	93	103	112	122	131	140	148	156	161	162	157	151	142	133	124	115
81	170	65	75	85	95	104	114	124	134	144	153	162	169	170	163	154	144	135	125	115
90	180	65	75	85	95	105	115	125	135	145	155	165	175	175	165	155	145	135	125	115

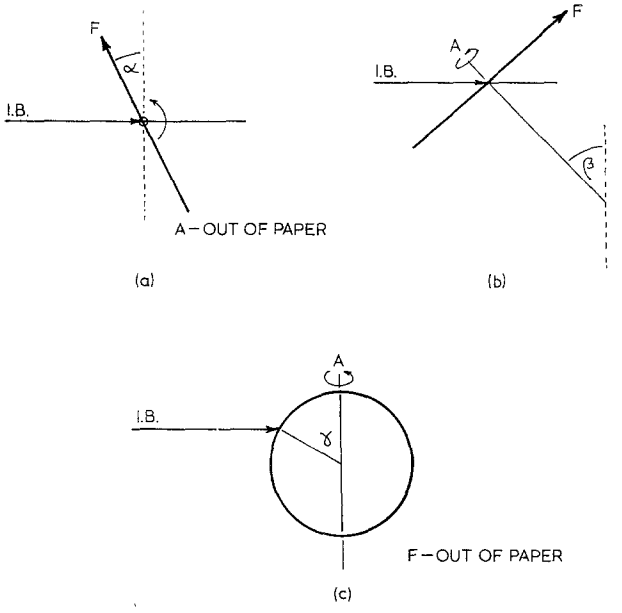

Figure 11 The geometry of ion bombardment of the fibres: (a) α defines the angular rotation of the fibre about the rotation axis, (b) β defines the inclination of the rotation axis to the vertical, (c) γ defines a line on the fibre surface parallel to the fibre axis. I.B. – ion beam, F – fibre axis, A – axis of rotation.

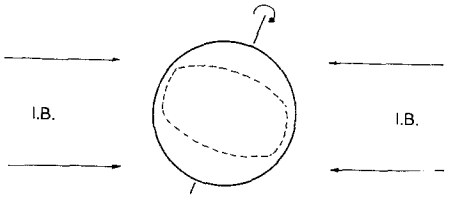

Figure 12 The change in shape of a rotated fibre under ion-bombardment. I.B. – ion beams. Dotted line shows fibre cross-section after some sputtering.

likely to prevent the development of striations and this is indeed the reason for rotating specimens being prepared for TEM. However, closer consideration shows that in the presence of rough ridges the situation is significantly altered. The striations arise because of inevitable fluctuations in the height of the axial ridges. At near glancing incidence the high parts of a ridge will be shielding the next (at present out of sight) ridge while low parts will permit sputtering of the next ridge. Clearly although the ion beam which is passing through the low part of the ridge is being scanned along the next ridge, this is occurring at a constant angular velocity and the maximum ion density (and hence sputtering rate) occurs perpendicular to the line of the ridges. This will lead to the development of striations perpendicular to the axial ridges and these will, in the early stages, be in areas of the fibre which are eroding relatively quickly and will consequently spread rapidly across the fibre.

5. Conclusions

The development of striations across the axes of fibres during ion-bombardment occurs by glancing-angle sputtering across the rough axial ridges. If it is necessary to remove the striations then the fibre must be polished smooth before bombardment begins. The angle of the striations to the fibre axis (ϕ) could be controlled by bombarding a static fibre at an appropriate value of α. If it is not necessary to remove the striations they should be recognized as arising from the mechanism of ion-bombardment, even when the specimen is rotated.

Acknowledgements

The author would like to thank Dr I. H. Wilson for his helpful comments and Mr M. Hepburn for experimental help.

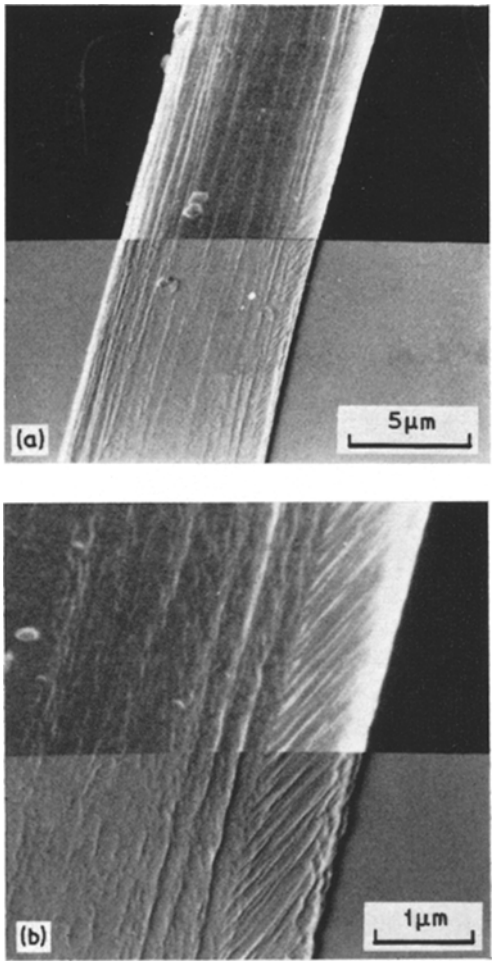

Figure 13 A PAN-based carbon fibre after stationary ion-bombardment at $\alpha = 90°$. Striations have formed at 25° to the fibre axis, as predicted in Table I. Scanning electron micrographs; top half is a secondary electron image, lower half is differentiated.

Appendix

The calculation of θ and ϕ, the angles of ion incidence on a rotating cylinder

The angle θ as defined in Fig. 9 is in this case the angle between the ion beam and the radius of the cylinder. We define our initial Cartesian co-ordinates with the origin at the centre of the cylinder, the ion beam along the x-axis and the fibre axis along the y-axis. A unit vector in the direction of the ion beam is then $(\bar{1}00)$. A simple way of calculating θ is to transform the co-ordinate system and to find the vector indices of the ion beam in a new system where the desired cylinder radius is along one of the axes. This is achieved by rotating the original co-ordinate system (x, y, z) by $\beta + (\pi/2)$ about the y-axis to give (x', y', z'), then by α about x' to give (x'', y'', z'') and finally γ about y'' to give a co-ordinate system (x''', y''', z''') in which x''' is the desired radius and y''' lies along the cylinder axis. θ is then the angle between x''' (i.e., $\bar{1}00$) and the co-ordinates of the ion beam in this new system $(u\ v\ w)$. Reference to Fig. 11 will make this clearer although a three-dimensional model is probably a greater help.

The necessary transformations can be written in matrix notation as

$$\begin{pmatrix} u \\ v \\ w \end{pmatrix} = \begin{pmatrix} \cos\gamma & 0 & \sin\gamma \\ 0 & 1 & 0 \\ -\sin\gamma & 0 & \cos\gamma \end{pmatrix} \begin{pmatrix} 1 & 0 & 0 \\ 0 & \cos\alpha & \sin\alpha \\ 0 & -\sin\alpha & \cos\alpha \end{pmatrix} \begin{pmatrix} \cos[\beta + (\pi/2)] & 0 & \sin[\beta + (\pi/2)] \\ 0 & 1 & 0 \\ -\sin[\beta + (\pi/2)] & 0 & \cos[\beta + (\pi/2)] \end{pmatrix} \begin{pmatrix} \bar{1} \\ 0 \\ 0 \end{pmatrix}$$

which simplifies to

$$\begin{pmatrix} u \\ v \\ w \end{pmatrix} = \begin{pmatrix} \sin\beta\cos\gamma + \cos\alpha\cos\beta\sin\gamma \\ \sin\gamma\cos\beta \\ -\sin\beta\sin\gamma + \cos\alpha\cos\beta\cos\gamma \end{pmatrix}.$$

The angle between $(\bar{1}00)$ and (uvw) is then given by

$$\cos\theta = -\sin\beta\cos\gamma - \cos\alpha\cos\beta\sin\gamma\,.$$

The angle ϕ is the angle between the ion beam and the fibre axis. This is conveniently expressed in a similar way as the angle between (010) and (pqr) where

$$\begin{pmatrix} p \\ q \\ r \end{pmatrix} = \begin{pmatrix} 1 & 0 & 0 \\ 0 & \cos\alpha & \sin\alpha \\ 0 & -\sin\alpha & \cos\alpha \end{pmatrix} \begin{pmatrix} -\sin\beta & 0 & \cos\beta \\ 0 & 1 & 0 \\ -\cos\beta & 0 & -\sin\beta \end{pmatrix} \begin{pmatrix} \bar{1} \\ 0 \\ 0 \end{pmatrix} = \begin{pmatrix} \sin\beta \\ \sin\alpha\cos\beta \\ \cos\alpha\cos\beta \end{pmatrix}.$$

Hence $\cos\phi = \sin\alpha\cos\beta\,.$

References

1. A. D. PEARSON and W. B. HARSELL, *Mat. Res. Bull.* **7** (1972) 567.
2. H. BACH, *J. Non-crystalline Solids* **3** (1970) 1.
3. D. J. BARBER, *J. Mater. Sci.* **5** (1970) 1.

4. P. J. GOODHEW, *J. Phys. EE.* **4** (1971) 392.
5. See, for example, M. NAVEZ, C. SELLA, and D. CHAPEROT in "Ionic Bombardment; theory and applications", ed. J. J. Trillat (Gordon and Breach, New York, 1964) p. 339.
6. G. K. WEHNER, *J. Appl. Phys.* **30** (1959) 1762.
7. A. D. G. STEWART and M. W. THOMPSON, *J. Mater. Sci.* **4** (1969) 56.
8. M. J. NOBES, J. S. COLLIGON, and G. CARTER, *ibid* **4** (1969) 730.
9. G. CARTER, J. S. COLLIGON, and M. J. NOBES, *ibid* **6** (1971) 115.
10. C. CATANA, J. S. COLLIGON, and G. CARTER, *ibid* **7** (1972) 467.
11. A. R. BAYLY, *ibid* **7** (1972) 404.
12. W. HAUFFE, *Phys. Stat. Sol.* (a) **4** (1971) 111.
13. J. V. SHARP, private communication.
14. P. J. GOODHEW, *Nature* **235** (1972) 437.
15. P. J. GOODHEW and M. J. HEPBURN, Proceedings of the Fifth European Cong. on Electron Microscopy, Manchester, 1972 (Institute of Physics, London 1972) p. 300.
16. R. A. COYLE, L. M. GILLIN, and B. J. WICKS, *J. Austral. Ceram. Soc.* **6** (1970) 29.
17. I. S. T. TSONG and D. J. BARBER, *J. Mater. Sci.* **7** (1972) 687.
18. I. H. WILSON and M. W. KIDD, *ibid* **6** (1971) 1362.

Received 24 July and accepted 25 September 1972.